



I S A V

**Journal of Theoretical and Applied
Vibration and Acoustics**

journal homepage: <http://tava.isav.ir>



Study on the dynamic behavior of cylindrical steel liquid storage tanks using finite element method

Mohsen Yazdanian^{a*}, Seyed Vahid Razavi^b, Mahmoud Mashal^c

^a Young Researchers and Elite Club, Ahvaz Branch, Islamic Azad University, Ahvaz, Iran

^b Department of Civil Engineering, Jundi-Shapur University of Technology, Dezful, Iran

^c Department of Irrigation Engineering, Aburaihan Campus, Tehran University, Tehran, Iran

ARTICLE INFO

Article history:

Received 28 January 2016

Received in revised form
15 June 2016

Accepted 19 June 2016

Available online 13 September
2016

Keywords:

CSTs

Height

Diameter

Earthquake

Time history

ABSTRACT

Dynamic behavior of ground supported cylindrical storage tanks (CST) is of crucial importance because of its applications in industrial complexes. Seismic behavior of tanks is greatly affected by the height to diameter ratio, fluid height and fluid type. Five CSTs with different height to diameter ratios, three CSTs with the same height and diameters but various fluid heights and one CST with two different fluid types are selected to determine the effect of height to diameter ratio, fluid heights, and fluid type on the seismic behavior of the tanks respectively. Static, modal, response spectrum, and time history analyses are used in this study for the selected CSTs using ANSYS finite element software. In the time history analysis method, the Tabas, Kobe and Cape Mendocino earthquake records have been utilized on the first five CSTs to ascertain the effect of height to diameter ratio and the Tabas earthquake record is used for the rest of CSTs. Results show that an increase in fluid height lead to a corresponding increase in the base shear. Based on observations, 100 percent increase in the diameter showed 63 percent increase in sloshing under the response spectrum and 70 percent under time history analyses. Based on static and response spectrum analyses, the highest values of displacements are obtained at the lowest part of the tanks, while in time history analysis, the highest is obtained at the top of the tanks. All analyses showed that the maximum stress occurred at the height of 1 to 2 meter from the bottom of the tanks.

©2016 Iranian Society of Acoustics and Vibration, All rights reserved.

1. Introduction

Cylindrical Storage Tanks (CSTs), as lifeline and strategically vital structures are usually used in petroleum industries, urban water infrastructures and nuclear water plants. CST is used in

* Corresponding Author.

E-mail address: m.yazdanian@iauahvaz.ac.ir (M. Yazdanian)

construction of storage tank for its simple design, cost efficiency and very thin perimeter walls (Bayraktar et al., 2010 [1]). Damages of CSTs besides disrupting vital infrastructures during a critical earthquake may lead to fire or environmental contaminations. These arise from the flammable storage liquid that can potentially affect the public safety (Shekari et al., 2010 [2]). The typical example of such disaster is the severe damages caused by the 1964 Niigata earthquake, with the reported extensive uncontrolled fire eruption in petroleum tanks which burned 286 houses in the adjacent area (Akatsuka and Kobayashi, 2010 [3]). The seismic behavior of storage tanks is a very complex subject. Fluid- structure interactions and variations in the liquid weight are two important issues that have to be taken into account in tank analysis modeling.

The most universally-used analytical model is the one developed by Housner (1963) [4]. The hydrodynamic pressure in Housner's model is separated into impulsive and convective components using lumped mass for the rigid tank. The results of the proposed model have been adopted with some changes in most of the existing codes and standards. For the first time, using the finite element method as a tool for estimating the seismic response of a cylindrical liquid storage tank is suggested by Edwards (1969) [5]. The proposed model in the finite element technique was capable of estimating the coupled interaction between the elastic tank perimeter wall and the stored liquid. Rosenblueth and Newmark (1971) [6] applied a lumped mass in their model using a rigid CST to investigate the seismic response. Yang (1976) [7], Veletos and Yang (1977) [8] are among others who considered the effects of tank's wall flexibility on the pressure distribution and corresponding forces in the liquid and the tank structure respectively. A simplified approach was developed by Veletsos and Kumar (1984) [9] to determine the effect of ground motion on cylindrical liquid storage tanks. Hamdan (2000) [10] investigated the behavior and design guidelines of CSTs that were subjected to ground motions and used field observations during past earthquakes with finite element analysis and published experimental results to assess the accuracy of design guidelines with special emphasis on Eurocode8 (2006) standard [11]. Virella et al. (2006) [12] studied the natural periods, mode shapes and dynamic response to ground motion of cylindrical tanks partially filled with a liquid. The contained liquid was modeled using the added mass formulation and acoustic liquid elements based on linear wave theory without any sloshing in waves. Ozdemir et al. (2010) [13] analyzed the CST using nonlinear methods for fluid-structure interaction with the help of the finite element method. Buratti and Tavano (2013) [14] investigated the dynamic buckling and seismic fragility of anchored cylindrical tanks using the added mass method. They analyzed the non-linear dynamic behavior of the tanks using a set of 40 recorded accelerograms by the finite element software. Ormeño et al (2015) [15] provided methods for seismic ground motion scaling in dynamic analysis of liquid storage tanks. Ruiz et al (2015) [16] proposed an efficient computational methodology for seismic analysis of liquid storage tanks. The proposed model was based on the theory of potential flow in which the Continuity equation is solved through the finite element method. Colombo and Almazan (2015) [17] assessed the efficiency of a specific energy dissipation procedure in two cylindrical tanks, including slender and broad tanks, by using the seismic reliability method.

Various studies have been undertaken to investigate the dynamic behavior of rectangular and cylindrical concrete tanks. Kianoush and Chen (2006) [18] investigated the impact of horizontal and vertical ground motion combination in concrete rectangular tank in a 2D space. The parameter of wall flexibility was also considered in the suggested method. Livaoglu et al. (2011)

[19] investigated the dynamic behavior of the backfill on rectangular tanks using the finite element method. They considered both the effects of liquid–structure and soil–structure interactions. Kianoush and Ghaemmaghami (2011) [20] investigated the effect of different earthquake frequency contents on the dynamic response of two CRSTs using the finite element method by regarding soil-liquid-tank interaction. They showed that the overall seismic behavior of the tank is governed by the impulsive component.

Various research works have been conducted on steel cylindrical tanks, although there are a number of evidences that these types of tanks are vulnerable against recurrence of severe earthquake. Recent studies have generally failed to focus on the effect of earthquake on various parameters. Instead, they have focused on a specific tank. The prime focus of this study is on the steel cylindrical tanks and a number of parameters such as the height to diameter ratio (H/D), fluid height to tank height ratio (h_1/H) and fluid types that have an effect on the vulnerability of tanks against earthquake. The lack of investigation, in the available literature, on the vibration or seismic behavior of tanks is the point elaborated by the current paper. Four different analyses including static, modal, response spectrum and time history analyses are conducted in order to make a comparative analysis possible. One of the distinctive methodological advantages of this study over the conventional methods is the inclusion of three earthquakes' components (longitudinal, transverse and vertical) into analytical considerations. This is an important issue for the subject under investigation which many studies have failed to consider as can be seen from the content of the published literature.

This paper has led to several new findings which are developed using different tank models with different configurations that are investigated under three different earthquake records incorporating liquid–structure interaction.

2. Mathematical model

In the Eulerian and Lagrangian methods, the governing fluid structure system equation is calculated using wave propagation through the fluid by assuming linear compressibility and inviscosity. The wave propagation equation through fluid is as follows (Zienkiewicz and Taylor, 2000 [21]):

$$\nabla^2 p = \frac{1}{c^2} \frac{\partial^2 p}{\partial t^2} \quad (1)$$

where p is the acoustic pressure in the fluid at time t and c is the acoustic wave speed. The continuity condition of the contained fluid in this theory is consisted of the boundary conditions of the contact interface between the tank body and the fluid as well as the fluid free surface. The fluid is assumed to be irrotational, incompressible and inviscid and also, it is assumed that there is no mean flow of the fluid. Furthermore, the linear theory of sloshing is utilized for the convective response of the contained liquid in the tank. The velocity of the pressure wave is assumed to be infinity in the small volume of containers. Hence, the wave equation of the fluid system can be written as follows in three-dimensional space by assuming an ideal fluid (Zienkiewicz and Taylor, 2000 [21], Moslemi and Kianoush, 2012 [22]):

$$\nabla^2 p(x, y, z, t) = 0 \quad (2)$$

in which $p = p(x, y, z, t)$ is the hydrodynamic pressure.

The hydrodynamic pressure p in this equation could be because of horizontal and vertical dynamic excitations of the tank walls and the floor. Dynamic motions at these boundaries are related to the hydrodynamic pressure in the fluid domain by defining proper boundary conditions along structure– fluid interfaces as follows.

$$\frac{\partial p(x, y, z, t)}{\partial n} = -\rho_l a_n(x, y, z, t) \quad (3)$$

or in matrix notation as:

$$\{\mathbf{n}\}^T (\{\mathbf{L}\}\mathbf{p}) = -\rho_l \{\mathbf{n}\}^T \left[\frac{\partial^2}{\partial t^2} \{\mathbf{u}\} \right] \quad (4)$$

where ρ_l is the liquid density, a_n is the acceleration component on the boundary along the normal direction n outward, $\{\mathbf{n}\}$ is the unit normal to the interface S , $\{\mathbf{u}\}$ is the displacement vector of the structure at the interface and t is the time.

The following boundary condition accounting for the sloshing effects can be written based on the small amplitude wave assumption on the fluid free surface.

$$\frac{1}{g} \frac{\partial^2 p}{\partial t^2} + \frac{\partial p}{\partial z} = 0 \quad (5)$$

in which, g represents the acceleration due to gravity and z is the vertical direction. By utilizing the boundary condition mentioned in Eq. (5), the convective pressure distribution within the fluid domain can be achieved. The mentioned boundary condition at the fluid free surface should be replaced with the following boundary condition which imposes zero impulsive pressure at the free surface by considering the impulsive component of the fluid response.

$$p(x, y, z, t) = 0 \quad (6)$$

$$\{\nabla \cdot (\cdot)\} = \{\mathbf{L}\}^T = \left[\frac{\partial}{\partial \mathbf{x}} \quad \frac{\partial}{\partial \mathbf{y}} \quad \frac{\partial}{\partial \mathbf{z}} \right] \quad (7)$$

$$\nabla(\cdot) = \{\mathbf{L}\} \quad (8)$$

Therefore, Eq. (1) can be rewritten as:

$$\nabla \cdot \nabla p = 0 \quad (9)$$

or in matrix notation as:

$$\{\mathbf{L}\}^T (\{\mathbf{L}\} \mathbf{p}) = \mathbf{0} \quad (10)$$

The discretized form for a multi degree of freedom system subjected to external dynamic forces can be defined as (Chopra, 2000 [23]):

$$[\mathbf{M}]\{\ddot{\mathbf{u}}\} + [\mathbf{C}]\{\dot{\mathbf{u}}\} + [\mathbf{K}]\{\mathbf{u}\} = \{\mathbf{f}^a\} \quad (11)$$

where $[\mathbf{M}]$ is the mass matrix of the system, $[\mathbf{C}]$ is the damping matrix of the system, $[\mathbf{K}]$ is stiffness matrix of the system, $\{\mathbf{u}\}$ is the displacement vector, $\{\dot{\mathbf{u}}\}$ is the velocity vector, $\{\ddot{\mathbf{u}}\}$ is the acceleration vector and $\{\mathbf{f}^a\}$ is the applied load vector.

The interaction between the tank structure and the contained fluid causes a hydrodynamic pressure which applies a force on the structure and thus creates structural motions produced by an effective fluid load. In order to obtain the structure-fluid coupling equations, $\{\mathbf{f}^a\}$ in Eq. (11) is consisted of the resultant of all other forces $\{\mathbf{f}_e\}$ and the fluid pressure load acting at the interface $\{\mathbf{f}_e^{pr}\}$. The following equations are introduced by Moslemi and Kianoush, 2012 [22]:

$$[\mathbf{M}_e]\{\ddot{\mathbf{u}}_e\} + [\mathbf{C}_e]\{\dot{\mathbf{u}}_e\} + [\mathbf{K}_e]\{\mathbf{u}_e\} = \{\mathbf{f}_e\} + \{\mathbf{f}_e^{pr}\} \quad (12)$$

The fluid pressure load acting at the structure-fluid interface can be calculated by integrating the pressure over the interface surface area as:

$$\{\mathbf{f}_e^{pr}\} = \int_s \{\mathbf{G}'\} \mathbf{p} \{\mathbf{n}\} d(\mathbf{s}) \quad (13)$$

in which $\{\mathbf{G}'\}$ is the shape function used to discretize the structural displacement components (obtained from the structural element), \mathbf{p} is the fluid pressure and $\{\mathbf{n}\}$ is the normal at the fluid boundary. Using the finite element approximating shape functions for the spatial variation of the fluid pressure, one can write:

$$\mathbf{p} = \{\mathbf{G}\}^T \{\mathbf{p}_e\} \quad (14)$$

in which $\{\mathbf{G}\}$ is the shape function for the fluid in pressure and $\{\mathbf{p}_e\}$ is the nodal pressure vector. Substituting Eq. (14) into Eq. (13) gives:

$$\{\mathbf{f}_e^{pr}\} = \int_s \{\mathbf{G}'\} \{\mathbf{G}\}^T \{\mathbf{n}\} d(\mathbf{s}) \{\mathbf{p}_e\} \quad (15)$$

The fluid pressure load can be defined as in Eq. (16) by definition of the coupling matrix $[\mathbf{R}_e]$ which relates the pressure of the fluid and the forces on the structure-fluid interface.

$$\{\mathbf{f}_e^{pr}\} = [\mathbf{R}_e] \{\mathbf{p}_e\} \quad (16)$$

By comparing Eqs. (15) and (16), the coupling matrix is found to be:

$$[\mathbf{R}_e]^T = \int_s \{\mathbf{G}'\} \{\mathbf{G}\}^T \{\mathbf{n}\} d(\mathbf{s}) \quad (17)$$

By substituting Eq. (16) into Eq. (12), the dynamic elemental equation of the structure can be written as:

$$[\mathbf{M}_e]\{\ddot{\mathbf{u}}_e\} + [\mathbf{C}_e]\{\dot{\mathbf{u}}_e\} + [\mathbf{K}_e]\{\mathbf{u}_e\} - [\mathbf{R}_e]\{\mathbf{p}_e\} = \{\mathbf{f}_e\} \quad (18)$$

3. Finite element solution

The motion equation, Eq. (11) and the wave equation, Eq. (1) have to be considered together in the finite element method to simulate the structure-fluid interaction problem.

The total hydrodynamic response can be calculated from the wave equation Eq. (1) as well as the proper boundary conditions mentioned in Eqs. (3) and (5). The impulsive part of the response can be found by replacing the boundary condition defined in Eq. (5) with the boundary condition in Eq. (6). Having obtained the total and impulsive response values, the convective response is the difference between these two values. Employing the finite element shape functions for the spatial variation of the displacement components within the structural domain, the following equation can be written (Moslemi and Kianoush, 2012 [22]):

$$\mathbf{u} = \{\mathbf{G}\}^T \{\mathbf{u}_e\} \quad (19)$$

In which, $\{\mathbf{u}_e\}$ is the nodal displacement vector component. For simplicity in deriving the equations, the following notation is introduced:

$$[\mathbf{C}] = \{\mathbf{L}\}\{\mathbf{G}\}^T \quad (20)$$

Finally, using the previously mentioned boundary conditions in finite element discretization, the discretized wave equation in matrix notation can be defined as:

$$[\mathbf{M}_e^p]\{\ddot{\mathbf{p}}_e\} + [\mathbf{K}_e^p]\{\mathbf{p}_e\} + \rho_l [\mathbf{R}_e]^T \{\ddot{\mathbf{u}}_e\} = \{\mathbf{0}\} \quad (21)$$

where:

$$[\mathbf{M}_e^p] = \frac{1}{g} \int_{fs} \{\mathbf{G}\}\{\mathbf{G}\}^T d(fs)$$

$$[\mathbf{K}_e^p] = \int_{vfe} [\mathbf{C}]^T [\mathbf{C}] d(vfe)$$

$$[\mathbf{R}_e] = \int_s \{\mathbf{G}\} \{\mathbf{n}\}^T \{\mathbf{G}'\}^T \mathbf{d}(\mathbf{s})$$

In the above equations, “ f_s ” and “ v_{fe} ” express the free surface and volume of the fluid element respectively. As mentioned before, s indicates the structure-fluid interface. The waste of energy due to fluid damping can be computed by adding a waste term to the above equation:

$$[\mathbf{M}_e^p] \{\ddot{\mathbf{p}}_e\} + [\mathbf{C}_e^p] \{\dot{\mathbf{p}}_e\} + [\mathbf{K}_e^p] \{\mathbf{p}_e\} + \rho_l [\mathbf{R}_e]^T \{\ddot{\mathbf{u}}_e\} = \{\mathbf{0}\} \quad (22)$$

in which $[\mathbf{C}_e^p]$ is the matrix representing the fluid damping. In this research, the classical damping system known as the Rayleigh damping (α and β) is applied for both the structural and fluid domains leading to a classical damping for the whole scheme. Alpha damping and Beta damping are applied to indicate Rayleigh damping constants α and β . The damping matrix within the fluid domain $[\mathbf{C}_e^p]$ contains two parts which are due to the impulsive and convective components of the stored fluid:

$$[\mathbf{C}_e^p] = \alpha [\mathbf{M}] + \beta [\mathbf{K}] + \sum_{i=1}^m [\mathbf{CF}_i] \quad (23)$$

α is defined based on the natural frequency of the primary sloshing mode and it is calculated for the damping due to the sloshing on the free surface of the tank liquid. β is defined based on the primary frequency of the tank and simulates the damping due to the impulsive part. As offered by the API 650 (2008) standard [24], the damping ratios of 2 percent and 0.5 percent are specified for the impulsive and convective parts respectively.

The time history response of the structure-fluid system is calculated using the direct integration method. By defining the displacement and hydrodynamic pressure at time increment i , the displacement and hydrodynamic pressure values at time increment $i+1$ can be calculated using the direct integration system. In this method, the step by step integration is applied directly to achieve the solution for the original equations of motion of the system. The finite difference expansions in the time interval Δt in the Newmark time integration method is used for the solution of Eq. (22). In the current research, an integration time step of 0.02s is applied to the systems. The ANSYS (2009) [25] software, as a general purpose computer code is utilized to perform the analyses (Moslemi and Kianoush, 2012) [22].

4. Case study modeling

Dynamic behavior of CSTs constructed on the ground as fluid storage facility is of great importance because of having many applications in industrial complexes and also in designing

codes which are developed based on their static behaviors. In this study, five CSTs with different height to diameter ratios (H/D) have been chosen to study the impact of height to diameter ratio on seismic behavior of tanks. Three tanks were selected with the same heights and diameters for the tanks but with different heights for the fluid ratio inside the tanks to study the impact of fluid height to tank height (h_1/H) on seismic behavior of the tanks. Moreover, to study the effect of the fluid type on seismic behavior of tanks, one of the tanks was filled with two different fluids. Mechanical properties of the fluid and the tank as input to the model are shown in Table 1. Table 2 shows the geometric characteristics of the tanks to investigate the impact of height to diameter ratio. For this purpose, five tanks were selected. The tanks' dimensions are selected so that all possible ratios of height to diameter are covered. The same free height is considered for each tank. Furthermore, the same wall material and the same fluid were considered in the tanks. In addition, three tanks were selected to study the impact of h_1/H on the seismic behavior of selected tanks. The geometric characteristics of the selected tanks are shown in Table 3. The properties of three tanks consist of the same wall material and fluid. All three tanks had the same height and diameter and the only parameter which is selected differed from others is the height of the fluid inside the tank. The impact of the fluid type on the seismic behavior of tanks was also investigated. The tank No.3 was selected which was filled with oil and water.

Table 1. Mechanical properties of the fluid and the tank

Materials properties	Density (kg/m ³)	Poisson's ratio	Young's modulus (GPa)	Bulk modulus (GPa)
Steel	7850	0.3	210	-
Fluid (water)	1000	-	-	2.07
Fluid (oil)	800	-	-	1.62

Table 2. The geometric characteristics of the tanks to investigate the impact of H/D

Tank No.	Height (m)	Diameter (m)	H / D	Shell thickness range (mm)
1	6	12	0.5	8-12
2	9.5	12	0.8	8-12
3	12	12	1	8-12
4	12	9.6	1.25	8-12
5	12	6	2	8-12

Table 3. The geometric characteristics of the tanks to investigate the impact of h_1/H

Tank No.	h_1/H	Diameter (m)	Height (m)	Shell thickness (mm)
6	0.87	12	12	8-12
7	0.5	12	12	8-12
8	0.25	12	12	8-12

5. Results and discussion

Four types of analysis i.e. static, modal, response spectrum, and time history had been performed. Tank No. 1 for empty and full fluid condition is illustrated in Fig. 1. Fig. 2 shows three tanks (No. 6, No. 7 and No. 8) which are modeled using the finite element software. First, static analysis was performed on all eight tanks and then, modal analysis, response spectrum analysis and time history analysis were conducted.

In the first step, static analysis was carried out and in this stage, the tanks were analyzed based on their weight and the hydrostatic pressure of the internal fluid. This analysis can be used in compound loading and also it can be used as a criterion for evaluation of the constructed model. The generated hydrostatic pressure causes annular tensile stresses in the tank wall. After modal analysis and determination of the main modes of tanks, response spectrum analysis was performed. A three components site design spectrum for area soil with moderate earthquake hazard has been selected. In the time history analysis, earthquake records of Tabas, Kobe and Cape Mendocino have been applied to five different tanks with various H/D ratios. Also, for the three tanks with different fluid heights and different fluids, the Tabas earthquake record is used.



Fig. 1: Finite element modeling of tank No.1 in empty and full conditions

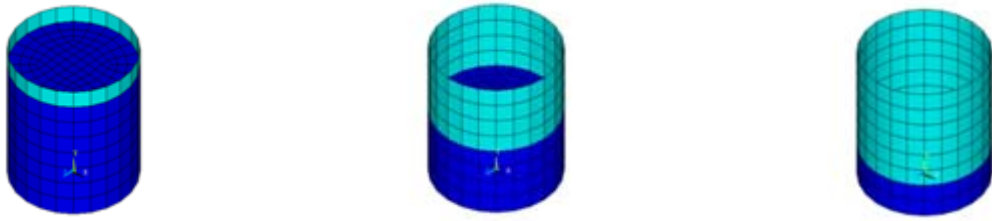


Fig. 2: Finite element modeling of tanks for three fluid height ratios

5.1. Modal analysis and validation

Natural frequencies and mode shapes of a tank are important parameters in the analysis of the tank. Determining these parameters in the first step can be very useful in interpreting the behavior of the tank. Convective and impulsive modes are the most important modes which have the maximum effective mass to account for the dynamic analysis. In addition, this analysis can be a starting point for other analyses such as the response spectrum analysis or the time history analysis. Fig. 3 illustrates two vibrational modes of the tank No.1. Tables 4 and 5 demonstrate the accuracy and validity of the finite element software result. In Table 4, the natural frequencies and convective and impulsive weights are compared with the analytical solutions calculated by the API standard. It can be seen that both natural frequencies and weights obtained from the finite element method are in good agreement with the API standard. Also, another verification method is shown in Table 5. To this end, some structural responses of an analytical model that was proposed in Ozdemir et al. (2010) [13] are compared with those obtained from the current finite element method. The tank model used in [13] has a radius of 1.83 m and a total height of 1.83 m. The tank is filled up to a height of 1.53 m water with a density of 1000 kg/m³. The tanks' shell was assumed to be aluminum with a density of 2700 kg/m³, the elastic modulus of 71.0 GPa and the yield stress of 100 MPa. In the numerical analysis, the horizontal component of the El Centro 1940 earthquake with 0.50 g peak acceleration was used.

Table 4. Natural frequencies of CSTs (Hz) and convective and impulsive weights of CSTs (Ton)

Tank No.	Convective mode (FEM)	Convective mode (API)	Impulsive mode (FEM)	Impulsive mode (API)	Convective weight (FEM)	Convective weight (API)	Impulsive weight (FEM)	Impulsive weight (API)
1	0.25	0.26	19.8	19.4	267.6	272.9	215.3	211.7
2	0.27	0.27	12.54	12.7	279.2	286.4	562.5	558.4
3	0.27	0.27	9.26	9.24	331.5	339	854.5	850
4	0.3	0.31	9.97	9.99	168.1	174.4	889.6	885.5
5	0.37	0.38	10.44	10.36	36.4	38	257.4	253.2
7	0.26	0.27	16.66	16.2	229.4	234.6	295.8	291.3
8	0.21	0.23	24.54	25.61	173.7	178.9	81.3	77.3

Table 5. Structural response of the tank model

Parameter	Ozdemir et al.	Current research
Max sloshing wave height (m)	0.09	0.09
Base shear (N)	4.62×10^4	4.61×10^4



Fig. 3: Illustration of mode shape for tank No. 1 from modal analysis

5.2. Effect of height to diameter ratio (H/D)

A summary of the main results from the static and response spectrum analyses is presented in Tables 6 and 7. The two tanks (No. 1 and No. 5) have the lowest displacements and tensile stresses in both static and response spectrum analyses. These two tanks have less fluid volume than the other three tanks and thus, tolerated less displacement and tensile stress values. The tank No. 3, with the highest volume of fluid among other tanks, has the highest displacement and tensile stress. In the tank No. 1, the maximum tensile stress occurred at the height of 1.5 m which is shown in Fig. 4, while in other cases, the maximum stress occurred at a height of 1.5 to 3 m. Regarding the wave height of tanks in Table 7, it is evident that the maximum wave height occurred in tanks No. 1, No. 2 and No. 3. This is due to having greater diameters in these tanks as compared with the other two ones. Fig. 5 shows the wave height of the tank No. 1. Displacement values obtained from time history analysis are shown in Table 8. It can be observed that the maximum displacement is related to the Tabas earthquake. The maximum and minimum displacements occurred in tanks No. 3 and No. 1 respectively. The wave height values obtained from time history analysis is more than the values obtained from response spectrum analysis. Table 8 presents the highest values of wave height in five tanks to investigate the effect of H/D . The Tabas earthquake has a higher PGA and this results in higher values in the analysis. The maximum wave height in the three tanks with $H/D = 0.5$, $H/D = 0.8$ and

$H/D = 1$ are higher than the two others. These three tanks have greater diameter and as a result, they show greater values of sloshing. This was previously discussed in the response spectrum analysis. Also, comparison of results show that, there is a huge difference between the results obtained from the time history analysis and the response spectrum analysis. This difference is due to the fact that the acceleration magnitude of the earthquakes which have been selected for time history analysis are higher than the spectrum which is calculated from the codes in response spectrum analysis. In the time history analysis, the tanks are excited using a realistic ground motion record, whereas in response spectrum analysis, the tanks are excited by a spectrum which is calculated from the codes and is not a suitable method when dynamic analysis needs to be considered.

Table 6. Comparison of the results obtained from static analysis

Tank No.	H/D	Maximum displacement (m)	Maximum tensile stress (MPa)
1	0.5	0.0009	16
2	0.8	0.0014	32.3
3	1	0.002	49.4
4	1.25	0.0014	38.8
5	2	0.0006	23.1

Table 7. Comparison of the results obtained from response spectrum analysis

Tank No.	H/D	Maximum displacement (m)	Maximum tensile stress (MPa)	Wave height (m)
1	0.5	0.0009	17.2	0.502
2	0.8	0.0015	33.2	0.528
3	1	0.003	68.6	0.524
4	1.25	0.0018	46.1	0.449
5	2	0.0018	26.6	0.319

Table 8. The maximum displacement and wave height obtained from time history

Earthquake name	H/D	Longitude displacement (m)	Vertically displacement (m)	Transverse displacement (m)	Wave height (m)
Tabas		0.0037	0.0005	0.0001	2.42
Kobe	0.5	0.001	0.0002	0.00009	1.24
Cape Mendocino		0.001	0.0002	0.00008	1.12
Tabas		0.012	0.002	0.0005	1.9
Kobe	0.8	0.005	0.001	0.0003	0.929
Cape Mendocino		0.004	0.001	0.0002	0.865
Tabas		0.089	0.677	0.166	2.41
Kobe	1	0.041	0.162	0.056	0.975
Cape Mendocino		0.029	0.131	0.05	.97
Tabas		0.019	0.005	0.001	2.048
Kobe	1.25	0.009	0.002	0.0006	0.95
Cape Mendocino		0.009	0.003	0.0008	0.91
Tabas		0.01	0.005	0.001	1.864
Kobe	2	0.008	0.003	0.0005	0.861
Cape Mendocino		0.005	0.004	0.0008	0.827

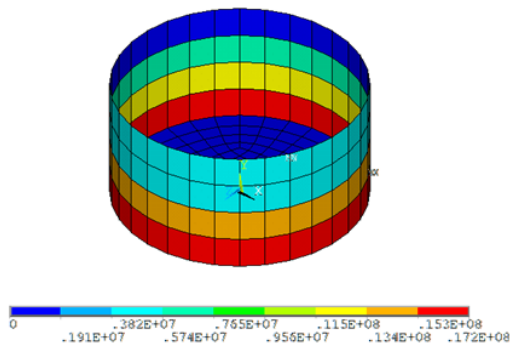


Fig. 4: Maximum tensile stress (Pa) in tank No. 1 wall

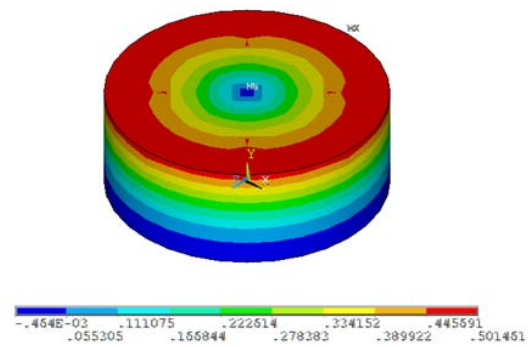


Fig. 5: Maximum wave height (m) in tank No. 1

In time history analysis, the earthquake records of Tabas, Kobe and Cape Mendocino have been applied to five different tanks with various H/D ratios. The results obtained from the maximum base shear are shown in Table 9. A more detailed look at this table shows that the maximum base shear values are obtained in the Tabas earthquake which is due to more peak ground acceleration (PGA) of the Tabas earthquake as compared with the other two records. Tank No. 3, with $H/D = 1$, shows a greater base shear than the other tanks and this is due to the fact that this tank has heavier weight than the other tanks. Also, the minimum value of base shear was obtained in tank No. 1 with $H/D = 0.5$. As mentioned previously, this tank has the lowest weight among all these five tanks. The maximum base shear response of the tank No. 1 with height to diameter ratio of 0.5 on the Tabas earthquake is presented in Fig. 6. In tank No. 1, the maximum base shear values along the longitudinal axis (X) and the transverse axis (Z) after the Tabas earthquake are 10.5 and 8.82 respectively.

Table 9. Maximum base shear obtained from time history analysis

Earthquake name	H/D	Longitudinal base shear (MN)	Transverse base shear (MN)
Tabas		1.31	1.16
Kobe	0.5	0.8	0.941
Cape Mendocino		1.23	1.23
Tabas		3.48	3.08
Kobe	0.8	1.81	2.42
Cape Mendocino		2.61	2.92
Tabas		9.23	7.48
Kobe	1	2.94	4.5
Cape Mendocino		5.23	5.13
Tabas		4.95	5.04
Kobe	1.25	2.09	2.97
Cape Mendocino		3.73	4.12
Tabas		2.08	2.21
Kobe	2	0.929	1.27
Cape Mendocino		1.51	1.64

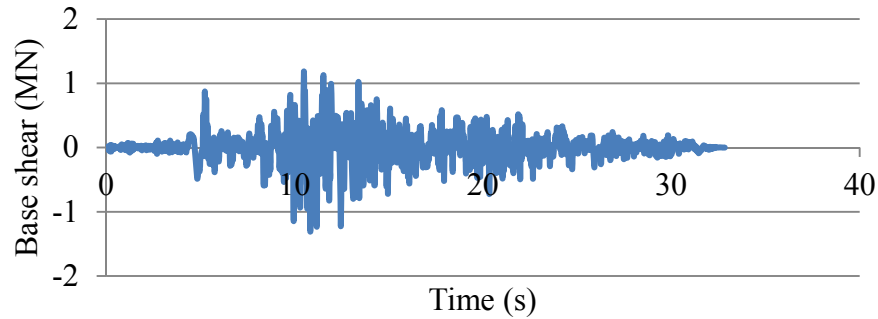


Fig. 6: The maximum base shear in the tank No. 1 ($H/D = 0.5$) for the Tabas earthquake along longitudinal axis

5.3. Effect of h_1/H

In the Tables 10 and 11, the main results of the static and response spectrum analyses are provided given three tanks for all three h_1/H ratios. Both tables indicate that the maximum displacements for tanks occurred when $h_1/H = 0.87$ while the lowest displacement was for the ratio as 0.25. Also, the values of tensile stress showed that the maximum tensile stress was determined when $h_1/H = 0.87$ and the minimum value of the tensile stress in the tank was for $h_1/H = 0.25$. The results show that an increase in the height of the fluid leads to an increase in the displacement and stress values. Comparison of results between the values of tensile stress obtained from the response spectrum and static analyses show that the highest difference between the two analyses occurs for the tank with $h_1/H = 0.87$. In addition, a comparison between the values of wave height for all three ratios shows that the maximum wave height occurred for the tank with $h_1/H = 0.87$, while the minimum wave height occurred for the tank with $h_1/H = 0.25$. This indicates that with increasing the fluid height, the wave height increases. Fig. 7 shows the maximum tensile stress for tanks in three different conditions. According to this figure, the maximum tensile stress occurred for the tank with $h_1/H = 0.87$ and 1.5 to 3 m height from the tank bottom and for the tank with $h_1/H = 0.25$ at 1.5 m from the bottom. A comparison among displacement and wave height values of three tanks in three h_1/H ratios are shown in Table 12. It can be seen from Table 12 that the maximum displacement in all three axes occurred in the tank with $h_1/H = 0.87$. A comparison between wave height values of the tanks for three states of filling obtained from time history analysis shows that the maximum wave height occurred in a tank with $h_1/H = 0.25$ with 2.59 m wave height, while the minimum height occurred in a tank with $h_1/H = 0.87$, with 2.4 m wave height. Comparison of the values from wave height indicates that there is a significant difference between values of wave height obtained from time history and response spectrum analyses. Furthermore, Fig. 8 shows liquid variation at one of the nodes on the fluid surface of the tank with $h_1/H = 0.87$.

Table 10. Comparison of the results obtained from static analysis

h_1/H	Maximum displacement (m)	Maximum tensile stress (MPa)
0.87	0.002	39.6
0.5	0.00088	19
0.25	0.00036	6.16

Table 11. Comparison of the results obtained from response spectrum analysis

h_1/H	Maximum displacement (m)	Maximum tensile stress (MPa)	Wave height (m)
0.87	0.002	48.3	0.527
0.5	0.00095	19.9	0.515
0.25	0.00044	7.43	0.447

Table 12. Maximum displacement and wave height under the Tabas record

h_1/H	Longitude displacement	Vertically displacement	Transverse displacement	Wave height (m)
0.87	0.028	0.004	0.001	2.4
0.5	0.006	0.0009	0.0002	2.44
0.25	0.002	0.0003	0.00005	2.59

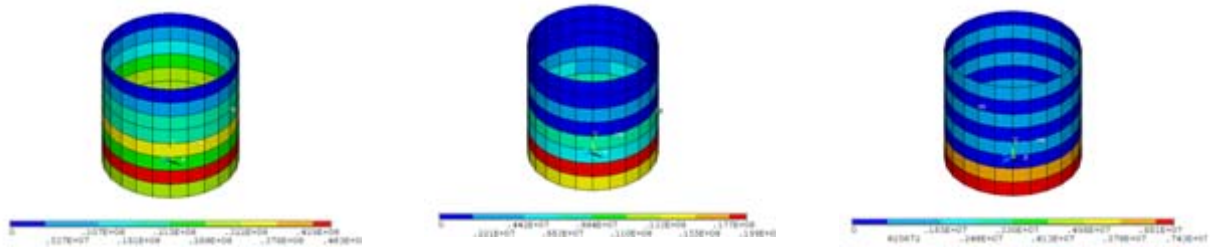


Fig. 7: The maximum tensile stress occurred in the tank wall in response spectrum analysis

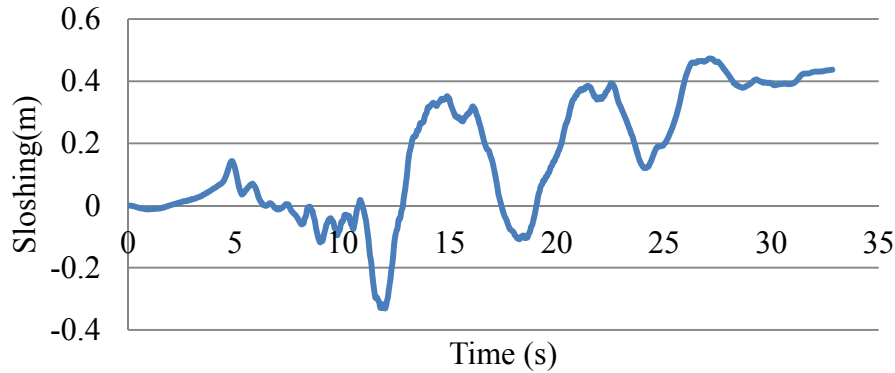


Fig. 8: A time history analysis response of sloshing in a tank with $h_1/H = 0.87$

Results of the maximum base shear obtained from time history analysis to examine the effect of h_1/H ratio are presented in table 13. For three tanks with different fluid heights, the Tabas earthquake record is used. A comparison among these results show that the maximum base shear occurred in a tank with $h_1/H = 0.87$, while the minimum occurred in a tank with $h_1/H = 0.25$. It should be noted that the value of the base shear in a tank with $h_1/H = 0.87$ is three times more than a tank with $h_1/H = 0.25$ and this shows an increase in weight lead to an increase in values of base shear. Fig. 9 shows the maximum base shear for a tank with $h_1/H = 0.5$. This graph shows that the maximum base shear in this tank occurred after 10.5 seconds, while at tank with $h_1/H = 0.25$ the maximum base shear occurred after 11.52 seconds of the Tabas earthquake. Also, in tank with $h_1/H = 0.87$ the maximum base shear is occurred after 10.04 seconds of the Tabas earthquake.

Table 13. The maximum base shear of tanks to examine the impact of h_1/H under the Tabas record

h_1/H	Longitudinal base shear (MN)	Transverse base shear (MN)
0.87	5.69	6.16
0.5	1.95	1.79
0.25	0.597	0.487

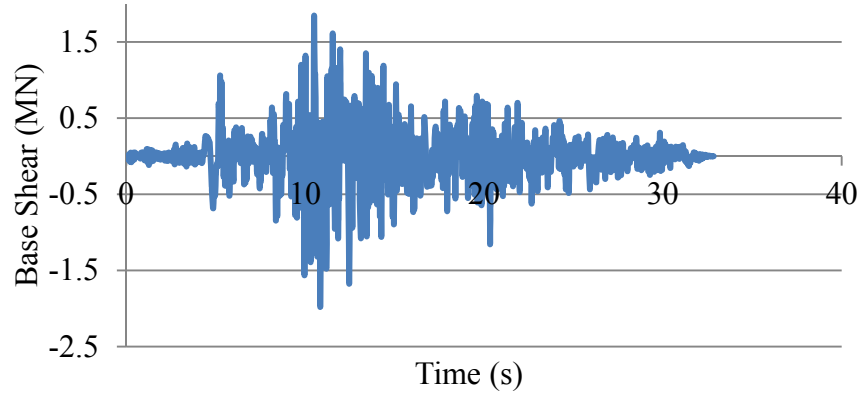


Fig. 9: The maximum base shear response of tank along the longitudinal axis in a tank with $h_1/H = 0.5$

5.4. Fluid type

Comparing the results obtained from the static and response spectrum analyses of tank No. 3 filled with two different fluids is presented in Tables 14 and 15. Both tables show that the two filled tanks of oil and water have almost the same displacement in static analysis, while in the response spectrum, due to wave height and also higher values of density, the tank filled with water experienced slightly higher values of displacement. Furthermore, in both analyses, the tank filled with water experienced higher tensile stress that is due to the higher density of water than oil and this difference is more highlighted in the response spectrum analysis. The results obtained from the displacements of the tanks filled with oil and water under the Tabas earthquake is shown in Table 16. This table shows that tank which is filled with water has higher displacements than the tank filled with oil and this was observed in response spectrum analysis. The difference is significantly increased in time history analysis. In addition, the wave height obtained for the tank filled with oil was a little bit higher due to its lower density than water in both time history and response spectrum analyses. The absolute maximum values of wave height obtained from time history analysis are higher than response spectrum analysis as it was expected. A comparison between the maximum base shear values of the two tanks filled with water and oil is shown in Table 17 and this indicates that the maximum base shear in the tank filled with water is more than the one filled with oil. This shows that an increase in weight results in an increase in the base shear as it was previously mentioned.

Table 14. Comparison of the results obtained from static analysis

Fluid Type	Maximum displacement (m)	Maximum tensile stress (MPa)
Oil	0.002	39.6
Water	0.002	49.4

Table 15. Comparison of the results obtained from response spectrum analysis

Fluid type	Maximum displacement (m)	Maximum tensile stress (MPa)	Wave height (m)
Oil	0.002	48.3	0.527
Water	0.003	68.6	0.524

Table 16. Maximum displacement and wave height under the Tabas record

Fluid type	Longitude displacement	Vertically displacement	Transverse displacement	Wave height (m)
Oil	0.028	0.004	0.001	2.5
Water	0.0898	0.677	0.166	2.41

Table 17. Maximum base shear of tanks under the Tabas record

Fluid type	Longitude base shear (MN)	Transverse base shear (MN)
Oil	5.69	6.16
Water	9.23	7.48

6. Conclusions

In this paper, five tanks were first modeled to determine the impact of height to diameter ratio. Furthermore, three tanks were used to study the impact of h_1/H on the seismic performance. Two tanks filled with oil and water were also compared to determine the impact of fluid type. The following items are the most important results obtained in this study:

- (1) In static analysis and response spectrum analysis, the results show that by a 130 percent increase in the tanks' volume ratio, there will be a corresponding 208 percent and 298 percent increase in the tensile stress for static and response spectrum analyses respectively. However, this was not the same in all tanks and the results showed that the ratio of height to diameter has a higher impact than the volume ratio on the obtained results. A 23 percent increase in the volume leads to a stress decline by 17 percent in static and 28 percent in response spectrum analyses which was due to the 56 percent rise in H/D .
- (2) Comparison of static and response spectrum analyses showed that the average increases in the results from static analysis to the response spectrum analysis for stresses and displacement values are 16.6 percent and 57.14 percent respectively.
- (3) By observing both the response spectrum analysis and time history analysis, it is found that an increase in the diameter of the tanks results in an increase in the sloshing. In other words, 100 percent increase in diameter showed 63 percent increase in sloshing under the response spectrum analysis and 70 percent under the time history analysis.

(4) Based on the results obtained from time history analysis, it was found that the earthquakes with greater PGA generally demonstrate greater base shear, displacement and wave height values.

(5) Results show that the average rate of displacement and wave height obtained from time history analysis are significantly greater as compared to those obtained from the response spectrum analysis. These average rises were about four times for wave heights and about ten times for displacements. These indicate the insufficiency of the response spectrum analysis to address such issues accurately and sufficiently.

(6) Studying the exact location of the maximum displacements and tensile stresses show that in static analysis, the maximum displacements generally occur at the height of 1 to 3 m from the bottom of the tanks, while in time history analysis, the maximum displacements occur at the highest part of the tanks. The tensile stress obtained from all analyses show that the maximum stress occurred at the height ranging between 1 to 2 m from the bottom of the tanks.

(7) Based on the results, it was found that a 3.5 times growth in the liquid height leads to a base shear increase by 9.5 times, displacement growth by 9 times, tensile stress increase by 6.5 times and wave height decrease by 8 percent.

(8) It was found that a 25 percent rise in the density of the fluid leads to 135 percent rise in displacements and a 33 percent rise in tensile stress values in the tank wall and a 62 percent in the values of base shear, while this amount of increase in density results in 3 percent decrease in wave height. It can therefore be concluded that it is important to identify the type of fluid in the design of the tanks in order to obtain valid and reliable results.

Acknowledgements

The authors would like to express their appreciation to the National Iranian South Oil Company for financial support provided to the authors and providing the necessary facilities to conduct this research project.

References

- [1] A. Bayraktar, B. Sevim, A.C. Altunışık, T. Türker, Effect of the model updating on the earthquake behavior of steel storage tanks, *Journal of Constructional Steel Research*, 66 (2010) 462-469.
- [2] M.R. Shekari, N. Khaji, M.T. Ahmadi, On the seismic behavior of cylindrical base-isolated liquid storage tanks excited by long-period ground motions, *Soil Dynamics and Earthquake Engineering*, 30 (2010) 968-980.
- [3] H. Akatsuka, H. Kobayashi, Fire of petroleum tank, etc. by Niigata earthquake, in, *Failure Knowledge Database*, Japan Science and Technology Agency, 2008.
- [4] G.W. Housner, The dynamic behavior of water tanks, *Bulletin of the seismological society of America*, 53 (1963) 381-387.
- [5] N.W. Edwards, A procedure for the dynamic analysis of thin walled cylindrical liquid storage tanks subjected to lateral ground motions, in, *University of Michigan, Ann Arbor, MI, USA*, 1969.
- [6] N.M. Newmark, E. Rosenblueth, *Fundamentals of earthquake engineering*, Prentice-Hall Civil engineering and engineering mechanics series, 12 (1971).

- [7] J.Y. Yang, Dynamic behavior of fluid-tank systems, in: Civil and Environmental Engineering Rice University, Houston, Texas, USA, 1976.
- [8] A.S. Veletsos, J. Auyang, Earthquake response of liquid storage tanks, in: Advances in Civil Engineering through Engineering Mechanics, ASCE, 1977, pp. 24.
- [9] A.S. Veletsos, A. Kumar, Dynamic response of vertically excited liquid storage tanks, in: Proceedings of the eighth world conference on earthquake engineering, San Francisco, California, USA, 1984, pp. 453-459.
- [10] F.H. Hamdan, Seismic behaviour of cylindrical steel liquid storage tanks, Journal of Constructional Steel Research, 53 (2000) 307-333.
- [11] E.C.f. Standardization, Eurocode 8: Design of structures for earthquake resistance, in: Part 4: Silos, tanks and pipelines EN 1998-4:2006 (E), 2006.
- [12] J.C. Virella, L.A. Godoy, L.E. Suárez, Fundamental modes of tank-liquid systems under horizontal motions, Engineering Structures, 28 (2006) 1450-1461.
- [13] Z. Ozdemir, M. Souli, Y.M. Fahjan, Application of nonlinear fluid–structure interaction methods to seismic analysis of anchored and unanchored tanks, Engineering Structures, 32 (2010) 409-423.
- [14] N. Buratti, M. Tavano, Dynamic buckling and seismic fragility of anchored steel tanks by the added mass method, Earthquake Engineering & Structural Dynamics, 43 (2014) 1-21.
- [15] M. Ormeño, T. Larkin, N. Chouw, Evaluation of seismic ground motion scaling procedures for linear time-history analysis of liquid storage tanks, Engineering Structures, 102 (2015) 266-277.
- [16] R.O. Ruiz, D. Lopez-Garcia, A.A. Taflanidis, An efficient computational procedure for the dynamic analysis of liquid storage tanks, Engineering Structures, 85 (2015) 206-218.
- [17] J.I. Colombo, J.L. Almazán, Seismic reliability of continuously supported steel wine storage tanks retrofitted with energy dissipation devices, Engineering Structures, 98 (2015) 201-211.
- [18] M.R. Kianoush, J.Z. Chen, Effect of vertical acceleration on response of concrete rectangular liquid storage tanks, Engineering Structures, 28 (2006) 704-715.
- [19] R. Livaoglu, T. Cakir, A. Dogangun, M. Aytakin, Effects of backfill on seismic behavior of rectangular tanks, Ocean Engineering, 38 (2011) 1161-1173.
- [20] M.R. Kianoush, A.R. Ghaemmaghami, The effect of earthquake frequency content on the seismic behavior of concrete rectangular liquid tanks using the finite element method incorporating soil–structure interaction, Engineering Structures, 33 (2011) 2186-2200.
- [21] O.C. Zienkiewicz, R.L. Taylor, The finite element method, Butterworth-heinemann, Linacre House, Jordan Hill, Oxford OX2 8DP, 2000.
- [22] M. Moslemi, M.R. Kianoush, Parametric study on dynamic behavior of cylindrical ground-supported tanks, Engineering Structures, 42 (2012) 214-230.
- [23] A.K. Chopra, Dynamics of structures, Prentice Hall New Jersey, 1995.
- [24] A.S. 650, Welded steel tanks for oil storage. 11th ed., American Petroleum Institute, Washington, D.C., USA., (2008).
- [25] ANSYS Release 12.0 Documentation, in, 2009.